The Company of
Biologists

METHODS & TECHNIQUES

In vivo continuous three-dimensional magnetic resonance microscopy: a study of metamorphosis in Carniolan worker honey bees (*Apis mellifera carnica*)

Aleš Mohorič[1,2], Janko Božič[3], Polona Mrak[3], Kaja Tušar[2], Chenyun Lin[3], Ana Sepe[1], Urša Mikac[1], Georgy Mikhaylov[1] and Igor Serša[1,*]

ABSTRACT

Three-dimensional (3D) magnetic resonance microscopy (MRM) is a modality of magnetic resonance imaging (MRI) optimized for the best resolution. Metamorphosis of the Carniolan worker honey bee (*Apis mellifera carnica*) was studied *in vivo* under controlled temperature and humidity conditions from sealed larvae until the emergence of an adult. The 3D images were analyzed by volume rendering and segmentation, enabling the analysis of the body, tracheal system and gastrointestinal tract through the time course of volume changes. Fat content sensitivity enabled the analysis of flight muscles transformation during the metamorphosis by the signal histogram and gray level co-occurrence matrix (GLCM). Although the transformation during metamorphosis is well known, MRM enables an alternative insight to this process, i.e. 3D *in vivo*, which has relatively high spatial and temporal resolutions. The developed methodology can easily be adapted for studying the metamorphosis of other insects or any other incremental biological process on a similar spatial and temporal scale.

KEY WORDS: Transformation of organs, Volumetric analysis, Flight muscle, GLCM image analysis

INTRODUCTION

Magnetic resonance microscopy (MRM), in comparison to the conventional magnetic resonance imaging (MRI), has a higher spatial resolution and uses almost identical imaging routines. With MRM, higher gradient strengths permit better resolution and faster imaging, and the stronger the magnetic field, the greater the signal-to-noise ratio (Callaghan, 1991). Their optimal water/lipid content and their size make insects one of the ideal samples for the MRM studies (Hart et al., 2003). Previously, studies on the morphologies of locusts (Gassner and Lohman, 1987), ladybirds (Geoghegan et al., 2000), honey bees (Tomanek et al., 1996), diving beetles (Wecker et al., 2002), fruit flies (Meme et al., 2013) and, more recently, stag beetles (Seo, 2018) have been reported. Several studies were also focused on the development of insects, e.g. in wasps (Chudek et al., 1996) and tobacco hornworms (Conner et al., 1988; Rowland and Goodman, 2016), or on the metamorphosis of Lepidoptera (Goodman et al., 1995) and silk larvae (Mapelli et al.,

1997). MRM efficiency has also been proven in the analysis of insect brains (Haddad et al., 2004; Michaelis et al., 2005; Watanabe et al., 2006) and the lipid content of the insects (Schilling et al., 2012). Another study reported on the parasite–host relationship in insects (Chudek et al., 1998).

In this feasibility study, the metamorphosis of the Carniolan worker honey bee (*Apis mellifera carnica*) from sealed larva up to the development of an adult was followed by the continuous three-dimensional (3D) MRM. The series of 3D images were analyzed to extract the information on transformation of the tracheal system, gastrointestinal tract and the muscles. Owing to its long duration and limited experimental time, the study was performed only on two specimens.

MATERIALS AND METHODS
Animal sample preparation

The experiment was performed in August 2018 and then in May 2020 on a single colony of Carniolan honey bees (*Apis mellifera carnica* Pollman 1879) in the Department of Biology, Biotechnical Faculty at the University of Ljubljana. On the day when the worker brood was capped, i.e. in mid-larval stage (day 0 in our study), a small section of it was removed from an experimental hive and immediately transported to the nearby MRI laboratory at the Jožef Stefan Institute. There, a single cell was carefully dissected from the brood, making sure that the cell remained capped and intact while its diameter was truncated to 10 mm, which was the diameter of the MRM probe in which the cell was then inserted (Fig. S1). Directly below the probe, an open container filled with humectant (saturated solution of $NaNO_2$ in water) was placed in order to maintain a constant humidity of $62\pm1\%$ during the entire experiment (Greenspan, 1977), and the continuous MRM scanning of sample was started. During the scanning, which lasted for several days, i.e. until the formation of an adult bee, the sample was left uninterrupted in the MRM system and the temperature was kept constant at 34°C to within 0.5°C tolerance with the MRM probe conditioning system. The conditioning system had no effect on the performance of the MRM system. Owing to the restricted availability of the MRM system and its long experimental duration, the analysis was performed only on two worker bee specimens. To gain additional insight into the intra-specimen variations, a similar experiment was undertaken with the drones of the same hive, which were scanned simultaneously by having multiple drones in the same imaging field of view. A section of freshly capped drone brood was inserted into a 30 mm MRM probe and the scanning was initiated immediately. The drone sample was continuously scanned until the formation of the adult drones such that the temperature and humidity control factors remained the same as in the case of the worker bee experiment.

[1]Jožef Stefan Institute, 1000 Ljubljana, Slovenia. [2]Faculty of Mathematics and Physics, University of Ljubljana, 1000 Ljubljana, Slovenia. [3]Department of Biology, Biotechnical Faculty, University of Ljubljana, 1000 Ljubljana, Slovenia.

*Author for correspondence (igor.sersa@ijs.si)

A.M., 0000-0001-6415-9019; J.B., 0000-0002-2546-478X; G.M., 0000-0003-1513-9825; I.S., 0000-0001-6799-3607

Magnetic resonance microscopy

The study was performed on an MRM system consisting of a 9.4 T (400 MHz proton frequency) high-resolution superconducting vertical-bore magnet (Jastec, Tokyo, Japan), a Bruker Micro 2.5 gradient system (Bruker, Ettlingen, Germany) and a Tecmag Redstone spectrometer (Tecmag, Houston, TX, USA). Worker and drone bees were scanned continuously using the 3D T_1-weighted spin-echo imaging sequence (Callaghan, 1991; Vlaardingerbroek and Boer, 1996). Scanning parameters for the worker bees were: field of view (FOV) $20 \times 10 \times 10$ mm^3, imaging matrix $256 \times 128 \times 128$ voxels, echo time (T_E) 2.2 ms, repetition time (T_R) 218 ms and number of signal averages 4. For the sample containing the drone bees, these parameters were: FOV $30 \times 30 \times 30$ mm^3, imaging matrix $256 \times 256 \times 256$ voxels, T_E 2.0 ms, T_R 219 ms and number of signal averages 2. Imaging resolution was equal to 78 and 117 µm for the bee and the drone experiment, respectively, in all three spatial directions. In contrast, the temporal resolution of the experiments (scan time for a single 3D image) for the worker bee and the drone samples were 4 and 8 h, respectively.

Microanatomy

Histological sections were prepared using one adult honey bee specimen that was previously subjected to MRM scanning. The entire body of the honey bee was fixed in 10% formaldehyde solution in phosphate buffered saline (PBS) in the decompression chamber at room temperature. After fixation and removal of the appendages, the specimen was dehydrated through an ascending series of ethanol and xylene, and was infiltrated with paraffin wax (Paraplast Plus, McCormick Scientific) at 60°C for 48 h. Dehydration and infiltration steps were performed in the decompression chamber. Afterwards, the specimen was embedded using a HistoCore Arcadia H paraffin embedding station (Leica, Wetzlar, Germany). Animal sagittal sections (7 µm) were prepared with a Leica RM2265 microtome, transferred to water on microscope slides and dried on a hot plate. After deparaffinization and rehydration, the sections were stained by a standard procedure of Hematoxylin & Eosin staining, using Weigert's iron hematoxylin, followed by dehydration and mounting. Imaging was performed with an AxioImager Z.1 light microscope (Zeiss, Oberkochen, Germany), equipped with an HRc Axiocam camera using Axiovision software.

Image processing and analysis

Three-dimensional MR images of the bee were digitally processed by the Fiji distribution (Schindelin et al., 2012) of the ImageJ digital image processing software (National Institutes of Health, Bethesda, MD, USA), which includes plugins for image segmentation, volume rendering and processing of image stacks. Volume-rendered images of the bee during metamorphosis from sealed larva to adult were calculated from the original 3D image sets. The tracheal system, characterized by signal voids inside the bee's body, was segmented using the thresholding method. Similarly, the gastrointestinal tract was characterized by the brighter envelope. Because the signal intensity of the gastrointestinal tract did not differ significantly from other surrounding tissues, the segmentation was done manually. Segmented images of the whole animal and its organs, i.e. tracheal system and gastrointestinal tract, were also used to calculate the corresponding volumes as a function of time. The length of the segmented gastrointestinal tract was calculated using Skeletonize3D and AnalyzeSkeleton ImageJ plugins, while tortuosity of the tract was calculated as the ratio of its length to the distance between its ends. Volumes of the bee and its organs were determined as the voxels with a signal intensity above the specified threshold. The volumetric uncertainty was estimated as the square root of the volume of superficial voxels. Single voxel volume was approximated to 4.77×10^{-4} mm^3 (calculated from FOV and imaging matrix).

The compositional analysis of the flight muscle as a function of time in two different ways was also performed. One method is the signal intensity histogram analysis of a 3D image segment of the muscle defined by a region of interest (ROI) with a size of $22 \times 16 \times 7$ pixels. This segment was analyzed from the transformation of pupal stage to the emergence of the adult. For each time point, the mean and standard deviation of the ROI signal were calculated.

The second method utilizes the gray level co-occurrence matrix (GLCM) analysis (Haralick et al., 1973) of the same image segment (ROI). GLCM has elements $p_{i,j}$ with values that correspond to the occurrences of pixels with intensity i having a pixel with intensity j in their neighborhood at a specified offset with respect to their position. GLCM is able to distinguish features in an image such as stripes or blocks from the noise even if they share the same average value and standard deviation. Each neighborhood-averaged GLCM matrix was represented by 11 second-order statistical texture features: (1) angular second moment (ASM), uniformity or energy; (2) entropy (ENT); (3) dissimilarity (DIS), (4) contrast (CON) or inertia; (5) inverse difference normalized (IDN); (6) correlation (COR); (7) inverse difference moment (IDM) or homogeneity; (8) variance (VAR); (9) cluster shade (SHA); (10) cluster prominence (PRO); and (11) maximum probability (MAX) (Yang et al., 2012). All of these statistical parameters were calculated for the ROI for most time points during development.

RESULTS

Metamorphosis from sealed larva to adult of the first worker bee specimen is depicted in a set of 3D T_1-weighted sequential images in the central sagittal plane for the selected times shown in Fig. 1A. In contrast, a complete set of both specimens is represented in Movie 1. Bright formations correspond to the fat-rich tissues that are used for the formation of other tissues during the first day of development. Prominent transformation of the specimen from larva to pupa occurred at day 3. After this transformation, all of the body parts and most of the internal organs are visible. During days 3 to 12, organs transform significantly. The gastrointestinal tract elongates up to day 5, then starts twisting up to day 7, becoming wider and growing towards the thorax section. A more detailed analysis of the thorax section shows myogenesis of flight muscles (Fig. S3). The muscles are initially brighter due to fatty inclusions which evolve into dark layered structure. Development of the brain along with the nervous system can also be seen. The size, orientation and shape of the head changes significantly during the development. Images at day 13 and later are blurred with both specimens because of an excessive motion of the bee trying to leave the cell. Three-dimensional images also enable volume rendering shown in Fig. 1B, Movie 1. The volume-rendered images enable the accurate visualization of the process showing all the changes of the external shape of the bee, such as development of extremities, head, thorax and abdomen.

Volume rendering of the segmented tracheal system enables the spatial visualization of the system (Fig. 1C, Movie 2). In the larval stage, rudiments of all the major airways exist which become wider and start branching further into narrow airways after the transformation into the pupal stage. Towards the end of the metamorphosis, the tracheal system becomes more complex and branched, and finer details can no longer be seen owing to the insufficient image resolution. The gastrointestinal tract (Fig. 1D, Movie 2) mainly shows rudiments of the tract in the larval state. Initially, a narrow and straight tube (up to day 2) becomes wider in course of time. During the
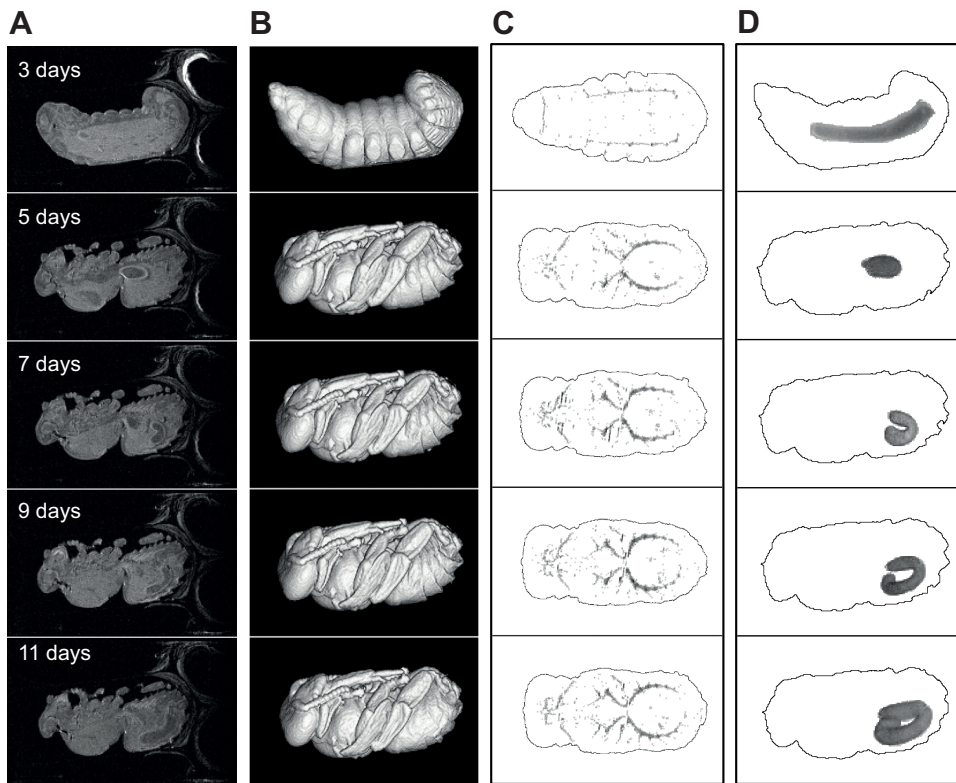
Fig. 1. Magnetic resonance microscopy of honey bee metamorphosis. (A) A subset of central slice images from 3D T_1-weighed image sets of a Carniolan honey bee (*Apis mellifera carnica*) acquired by sequential magnetic resonance microscopy during the development at selected times (left column). (B) Volume-rendered images of the honey bee at selected times of development. (C) Development of the tracheal system shown in the coronal (top–bottom) view. Images are a result of segmentation of airwaves followed by volume rendering. An outline of the bee is superimposed onto the image. (D) Development of the gastrointestinal tract shown in the sagittal (right–left) view. Images are a result of segmentation of the gastrointestinal tract followed by volume rendering. An outline of the bee is superimposed onto the image.

transformation from larva to pupa (day 3 and 4 h), the tube curves and the segmented stomodeum and midgut section of the gastrointestinal tract can be seen on the corresponding image, while the later images show only the stomodeum or the midgut because of insufficient contrast for reliable segmentation. Stomodeum is then pushed from thorax into the abdomen, where it starts forming the honey stomach. These observations correspond well with the original description by Snodgrass (Snodgrass, 1956). No curvature of the stomodeum is observed until day 5. After that, the midgut starts U-shaping (day 7) and finally C-shaping.

Fig. 2 shows graphs of average volumes with standard errors of the worker bee and some of its organs during the metamorphosis from sealed larva to adult. The total volume of the bee (Fig. 2A) first decreases and then sharply increases, coinciding with the transition from larva to pupa. From then onward, a relatively steady decrease is observed. The final average volume of the bees at the end of the metamorphosis is equal to 118 ± 18 mm^3. The volume of the tracheal system (Fig. 2B) practically triples after the transformation from larva to pupa, following almost steady growth until the end. After day 9, a moderate decline in the volume of the tracheal system is observed. This correlates with the narrow growth of major airways. The volume of the gastrointestinal tract (Fig. 2C) increases rapidly just before the transition from larva to pupa. After the transition, the volume decreases and remains practically unchanged until day 9. From then onward, the growth is considerable again until the end of metamorphosis. Most of the growth of the honey stomach occurs in the first 5 days after the transition from larva to pupa. From the graph of the bee's gastrointestinal tract tortuosity as a function of time (Fig. 2D), it can be seen that the tortuosity was close to 1 until day 5, when it started increasing until day 10 and was stabilized at a value of 8 during the emergence of the adult.

The sensitivity of MRI to the structural and compositional tissue changes also enables the analysis of flight muscles. A segment of the flight muscle of the worker bee specimens (Fig. 3A) was analyzed using image signal intensity histogram analysis. Measured histograms are shown in Fig. S3A, while the graph of the flight muscle's mean signal intensity and its standard deviation as a function of time is shown in Fig. 3B. The histograms measured in 1 day intervals exhibit a normal distribution with changing means and widths. Initially, the high mean intensity (blue curve) decreases at day 4, recovers until day 8 and gradually decreases until day 12. The corresponding standard deviation (orange curve) reaches the highest value at day 4, decreases until day 6 and is relatively constant from then onwards. The high values of the mean signal suggest a higher accumulation of fat. The decrease indicates change in the muscle composition towards the low fat content. The increase in the signal's standard deviation found soon after the transformation from larva to pupa at day 4 suggests the beginning of muscle transformation in which fat is used to build the muscle. Results of the muscle structure analysis in Fig. 3C are shown by GLCM maps that correspond to T_1-weighted images of flight muscle ROIs in Fig. 3A at three different stages of metamorphosis. The GLCM maps have distinct shift of distribution peak and also marked dependence on time of some second-order statistical texture features derived from the GLCM maps: correlation (COR), cluster shade (SHA), cluster prominence (PRO) and angular second moment (ASM). Time dependencies of features ASM, COR and SHA are shown in Fig. 3C, while time dependencies of remaining and less distinctive features are shown in Fig S3B.

DISCUSSION

The 3D MRM method was found to be efficient in the assessment of morphological and compositional changes, and allowed the undisturbed analysis of the same specimen throughout the process of metamorphosis from sealed larva to an adult. Frequent scanning (more than 80 sequential 3D images) did not affect the course of metamorphosis.

The right ambient conditions are essential for the vitality of the bee and its undisturbed development. Metamorphosis from larva to
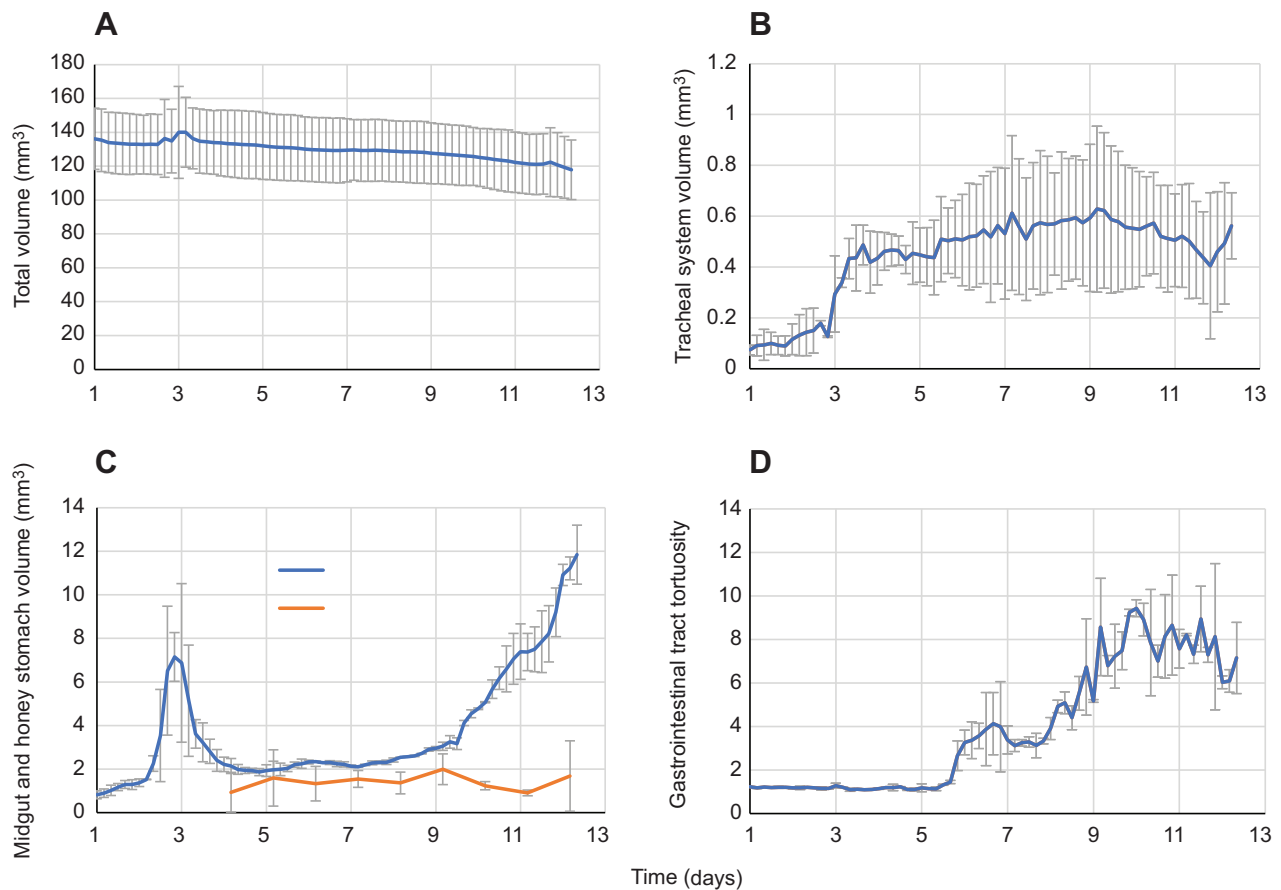
Fig. 2. Volume of a honey bee and its organs during metamorphosis. Time courses of (A) total insect volume, (B) tracheal system volume, (C) midgut and honey stomach volumes, as well as of (D) gastrointestinal tract tortuosity, which helps elucidate gastrointestinal tract shaping during the metamorphosis. Graphs, shown by average value curve and standard deviation of the measured points, were obtained as a result of statistical analysis of two summer worker bee specimens of the same hive.

adult took on average 12.5 days. The reduction of total volume by 13% (shown in Fig. 2A) can be explained by the use of nutrients for the organ build-up. Sub-optimal ambient conditions could also contribute to the deviations from the expected development dynamics, with variability also present between the specimens. The experiment with parallel imaging of drones in Fig. S2 indicated that variations of up to 10% in the volume of the insect body and its organs can be expected among the different specimens. These factors explain some anomalies in the development of organs, e.g. the decrease of the tracheal system volume after day 9. In the tracheal system, only the major sacks can be seen in the MR images owing to limited resolution. Major tracheal sacks additionally differentiate at the ends and could not be detected. Insufficient contrast between some sections of gastrointestinal tract and the surrounding tissues prevents a complete segmentation of the gastrointestinal tract and yields underestimated gastrointestinal tract volume.

Microscopic computed tomography (micro CT) is an alternative imaging method with higher spatial resolution, but it is not that efficient in distinguishing different soft tissues. However, it is also harmful owing to X-ray radiation. This method has been used previously for studying insect metamorphosis (Helm et al., 2018; Lowe et al., 2013; Martín-Vega et al., 2017) with parallel sample scans in a shorter time frame as compared with our method, which, however, has six times better temporal resolution. Problems such as blurring associated with the motion of the bee can be seen owing to

longer 3D scanning time during the larval stage and some phases of the late pupal stage. However, most changes during development were sufficiently slow to not affect the image quality by motion artifacts. Absence of motion artifact in the image taken before and then after the transformation from larva to pupa indicates that the transformation was completed in less than a frame time, i.e. less than 4 h. According to some previous studies, as in case of *Calliphora vicina* (Hall et al., 2017), the transformation took less than 2 h.

Comparison of MRM with micro CT performed on the winter worker bee (Fig. S4A,B) and of MRM with microanatomy on the summer worker bee (second specimen, Fig. S4C,D) confirms that the structures visualized by MRM are identical to those seen by micro CT and microanatomy, which has superb contrast and resolution and can be considered as a reference standard. In microanatomical images, fine structures can be observed which can help to better identify the anatomical parts on the corresponding MRM image. Conversely, MRM images can give an insight into the immediate original state of structures, especially on the shape and content of the lumen in parts of the digestive system such as the rectum. MRM analysis is also free of possible artifacts that are due to organ deformations and washing out of the lumen content, which can occur during histological sample preparation. In the experiment on the winter bee, the abdomen section appears in the MRM image much brighter than the head and thorax sections. This is because T_1-weighted MRM is sensitive to the fat content and winter bees have more fats in the abdominal section. Sensitivity of this method to fat-rich tissues enables morphological
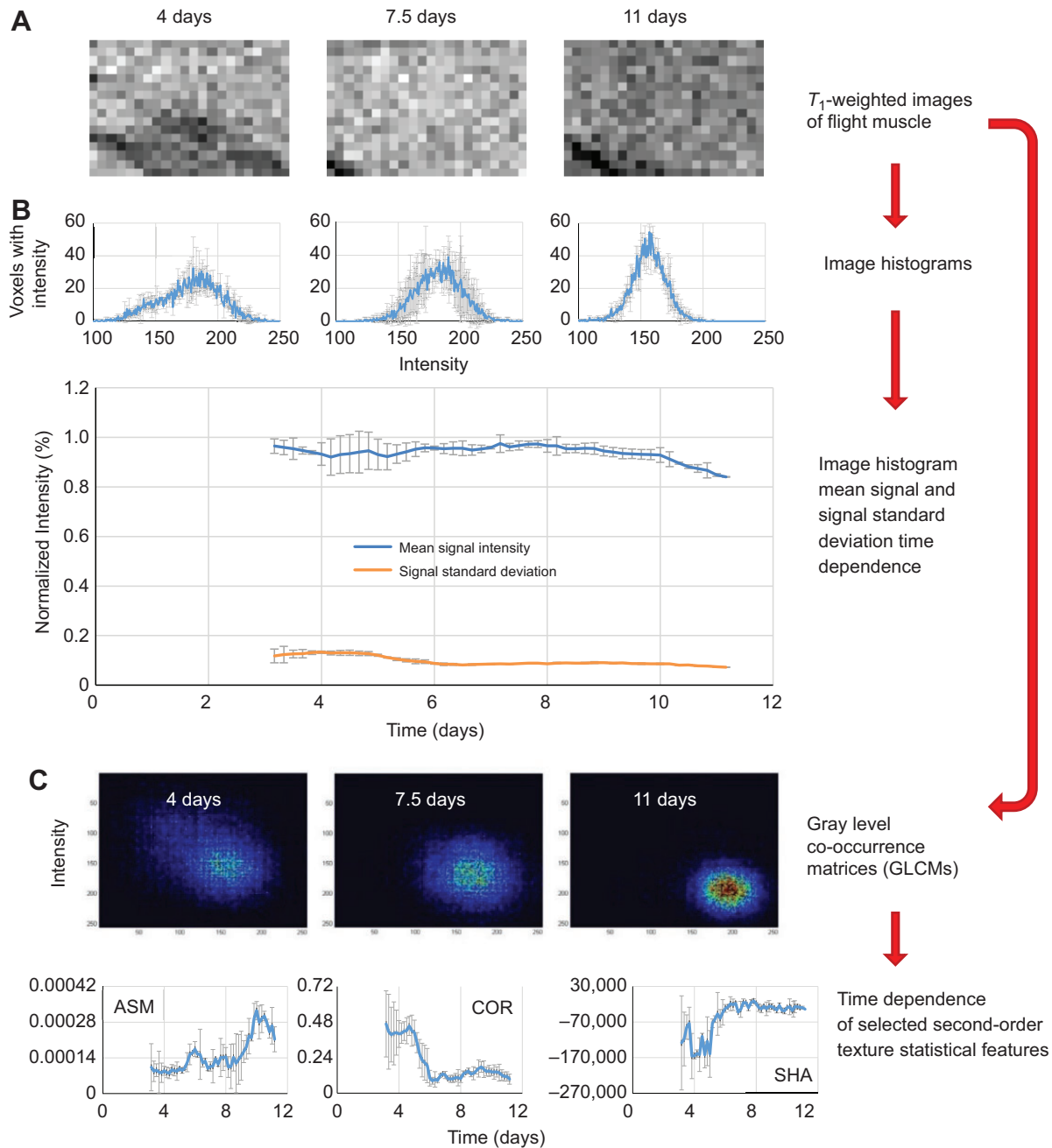
Fig. 3. Analysis of flight muscle transformation during honey bee metamorphisms. (A) The selected region of interest (ROI) within the flight muscle of worker bees is analyzed at different time points of the metamorphosis by (B) image signal histograms and (C) gray level co-occurrence matrices (GLCMs). (B) Time course graphs of the histogram mean and standard deviation reveal transformation of the flight muscle composition from the initial fat-rich to the final low fat. (C) Structural changes of the selected ROI within the flight muscle were detected by GLCM analysis. From the corresponding GLCM maps were derived time courses of all 11 second-order statistical texture features, only angular second moment (ASM), correlation (COR) and cluster shade (SHA) are shown, which have a marked time dependence.

visualization of different sections, and the compositional analysis, e.g. flight muscle analysis in Fig. 3, shows a transformation from fat-rich to low-fat containing tissues. Similar analysis could be performed on other organs that may undergo a substantial transformation, e.g. brains (Haddad et al., 2004).

There are several other possibilities of employing the presented 3D MRM method in other studies on the insects. For example, it would also be very interesting to investigate metamorphosis from egg to larval stage by MRM. In this study, we did not follow metamorphosis during first 9 days, i.e. from laid egg to sealed larva.

Another interesting topic is insect–parasite interactions, for example between honey bees and *Varroa* mites (Rosenkranz et al., 2010). MRI is quite a capable modality for this type of study (Chudek et al., 1998). It enables long observation times, is harmless and would have very little or almost no effect on this interaction.

In conclusion, the present study shows that MRM is a powerful tool for the analysis of morphological and compositional changes during the metamorphosis in insects. Unlike many other imaging modalities, MRM is harmless, which enables continuous scanning on the same specimen for a longer period of time. Clearly, MRM is

an ideal tool for studying insect development and other incremental biological processes on a similar spatial and temporal scale, provided the prolonged scanning time and restricted availability is not an issue.

Supplementary information
Supplementary information available online at
https://jeb.biologists.org/lookup/doi/10.1242/jeb.225250.supplemental

References

Callaghan, P. T. (1991). *Principles of Nuclear Magnetic Resonance Microscopy*. Oxford: Oxford University Press.

Chudek, J. A., Crook, A. M. E., Hubbard, S. F. and Hunter, G. (1996). Nuclear magnetic resonance microscopy of the development of the parasitoid wasp *Venturia canescens* within its host moth *Plodia interpunctella*. *Magn. Reson. Imaging* 14, 679-686. doi:10.1016/0730-725X(96)02104-2

Chudek, J. A., Hunter, G., MacKay, R. L., Moritz, S., Birch, A. N. E., Geoghegan, I. E., McNicol, R. J. and Majurs, M. E. N. (1998). MRM, an alternative approach to the study of host/parasitoid relationships in insects. In *Spatially Resolved Magnetic Resonance* (ed. P. Blümler, B. Blümich, R. Botto and E. Fukushima), pp. 467-471. Weinheim: Wiley-VCH.

Conner, W. E., Johnson, G. A., Cofer, G. P. and Dittrich, K. (1988). Magnetic resonance microscopy: in vivo sectioning of a developing insect. *Experientia* 44, 11-12. doi:10.1007/BF01960223

Gassner, G. and Lohman, J. A. B. (1987). Combined proton NMR imaging and spectral analysis of locust embryonic development. *Proc. Natl. Acad. Sci. USA* 84, 5297-5300. doi:10.1073/pnas.84.15.5297

Geoghegan, I. E., Chudek, J. A., Mackay, R. L., Lowe, C., Moritz, S., Mcnicol, R. J., Birch, A. N. E., Hunter, G. and Majurs, M. E. N. (2000). Study of anatomical changes in *Coccinella septempunctata* (Coleoptera: Coccinellidae) induced by diet and by infection with the larva of *Dinocampus coccinellae* (Hymenoptera: Braconidae) using magnetic resonance microimaging. *Eur. J. Entomol.* 97, 457-461. doi:10.14411/eje.2000.070

Goodman, B. A., Gordon, S. C., Chudek, J. A., Hunter, G. and Woodford, J. A. T. (1995). Nuclear-magnetic-resonance microscopy as a noninvasive tool to study the development of lepidopteran pupae. *J. Insect Physiol.* 41, 419-424. doi:10.1016/0022-1910(94)00115-W

Greenspan, L. (1977). Humidity fixed-points of binary saturated aqueous solutions. *J. Res. Nat. Inst. Stand. A* 81, 89-96. doi:10.6028/jres.081A.011

Haddad, D., Schaupp, F., Brandt, R., Manz, G., Menzel, R. and Haase, A. (2004). NMR imaging of the honeybee brain. *J. Insect Sci.* 4, 7. doi:10.1093/jis/4.1.7

Hall, M. J. R., Simonsen, T. J. and Martín-Vega, D. (2017). The 'dance' of life: visualizing metamorphosis during pupation in the blow fly *Calliphora vicina* by X-ray video imaging and micro-computed tomography. *R. Soc. Open. Sci.* 4, 160699. doi:10.1098/rsos.160699

Haralick, R. M., Shanmugam, K. and Dinstein, I. H. (1973). Textural features for image classification. *IEEE Trans. Syst. Man Cybern.* Smc3, 610-621. doi:10.1109/TSMC.1973.4309314

Hart, A. G., Bowtell, R. W., Kockenberger, W., Wenseleers, T. and Ratnieks, F. L. W. (2003). Magnetic resonance imaging in entomology: a critical review. *J. Insect Sci.* 3, 5. doi:10.1673/031.003.0501

Helm, B. R., Payne, S., Rinehart, J. P., Yocum, G. D., Bowsher, J. H. and Greenlee, K. J. (2018). Micro-computed tomography of pupal metamorphosis in the solitary bee *Megachile rotundata*. *Arthropod Struct. Dev.* 47, 521-528. doi:10.1016/j.asd.2018.05.001

Lowe, T., Garwood, R. J., Simonsen, T. J., Bradley, R. S. and Withers, P. J. (2013). Metamorphosis revealed: time-lapse three-dimensional imaging inside a living chrysalis. *J. R. Soc. Interface* 10, 20130304. doi:10.1098/rsif.2013.0304

Mapelli, M., Greco, F., Gussoni, M., Consonni, R. and Zetta, L. (1997). Application of NMR microscopy to the morphological study of the silkworm, *Bombyx mori* during its metamorphosis. *Magn. Reson. Imaging* 15, 693-700. doi:10.1016/S0730-725X(97)00006-4

Martín-Vega, D., Simonsen, T. J., Wicklein, M. and Hall, M. J. R. (2017). Age estimation during the blow fly intra-puparial period: a qualitative and quantitative approach using micro-computed tomography. *Int. J. Legal Med.* 131, 1429-1448. doi:10.1007/s00414-017-1598-2

Meme, S., Joudiou, N., Szeremeta, F., Mispelter, J., Louat, F., Decoville, M., Locker, D. and Beloeil, J.-C. (2013). In vivo magnetic resonance microscopy of Drosophilae at 9.4 T. *Magn. Reson. Imaging* 31, 109-119. doi:10.1016/j.mri.2012.06.019

Michaelis, T., Watanabe, T., Natt, O., Boretius, S., Frahm, J., Utz, S. and Schachtner, J. (2005). In vivo 3D MRI of insect brain: cerebral development during metamorphosis of *Manduca sexta*. *Neuroimage* 24, 596-602. doi:10.1016/j.neuroimage.2004.08.048

Rosenkranz, P., Aumeier, P. and Ziegelmann, B. (2010). Biology and control of *Varroa destructor*. *J. Invertebr. Pathol.* 103 Suppl. 1, S96-S119. doi:10.1016/j.jip.2009.07.016

Rowland, I. J. and Goodman, W. G. (2016). Magnetic resonance imaging of alimentary tract development in manduca sexta. *PLoS ONE* 11, e0157124. doi:10.1371/journal.pone.0157124

Schilling, F., Dworschak, K., Schopf, R., Kuhn, R., Glaser, S. J. and Haase, A. (2012). Non-invasive lipid measurement in living insects using NMR microscopy. *J. Exp. Biol.* 215, 3137-3141. doi:10.1242/jeb.071209

Schindelin, J., Arganda-Carreras, I., Frise, E., Kaynig, V., Longair, M., Pietzsch, T., Preibisch, S., Rueden, C., Saalfeld, S., Schmid, B. et al. (2012). Fiji: an open-source platform for biological-image analysis. *Nat. Methods* 9, 676-682. doi:10.1038/nmeth.2019

Seo, Y. (2018). High spatial resolution magnetic resonance imaging of insects covered with a hard exoskeleton. *Concept. Magn. Reson. B* 48b, e21366. doi:10.1002/cmr.b.21366

Snodgrass, R. E. (1956). *Anatomy of the Honey Bee*. Ithaca: Comstock Publishing Associates.

Tomanek, B., Jasinski, A., Sulek, Z., Muszynska, J., Kulinowski, P., Kwiecinski, S., Krzyzak, A., Skorka, T. Kibinski, J. (1996). Magnetic resonance microscopy of internal structure of drone and queen honey bees. *J. Apicult. Res.* 35, 3-9. doi:10.1080/00218839.1996.11100907

Vlaardingerbroek, M. T. and Boer, J. A. d. (1996). *Magnetic Resonance Imaging: Theory and Practice*. Berlin: Springer.

Watanabe, T., Schachtner, J., Krizan, M., Boretius, S., Frahm, J. and Michaelis, T. (2006). Manganese-enhanced 3D MRI of established and disrupted synaptic activity in the developing insect brain *in vivo*. *J. Neurosci. Methods* 158, 50-55. doi:10.1016/j.jneumeth.2006.05.012

Wecker, S., Hörnschemeyer, T. and Hoehn, M. (2002). Investigation of insect morphology by MRI: Assessment of spatial and temporal resolution. *Magn. Reson. Imaging* 20, 105-111. doi:10.1016/S0730-725X(01)00445-3

Yang, X. F., Tridandapani, S., Beitler, J. J., Yu, D. S., Yoshida, E. J., Curran, W. J. and Liu, T. (2012). Ultrasound GLCM texture analysis of radiation-induced parotid-gland injury in head-and-neck cancer radiotherapy: an *in vivo* study of late toxicity. *Med. Phys.* 39, 5732-5739. doi:10.1118/1.4747526
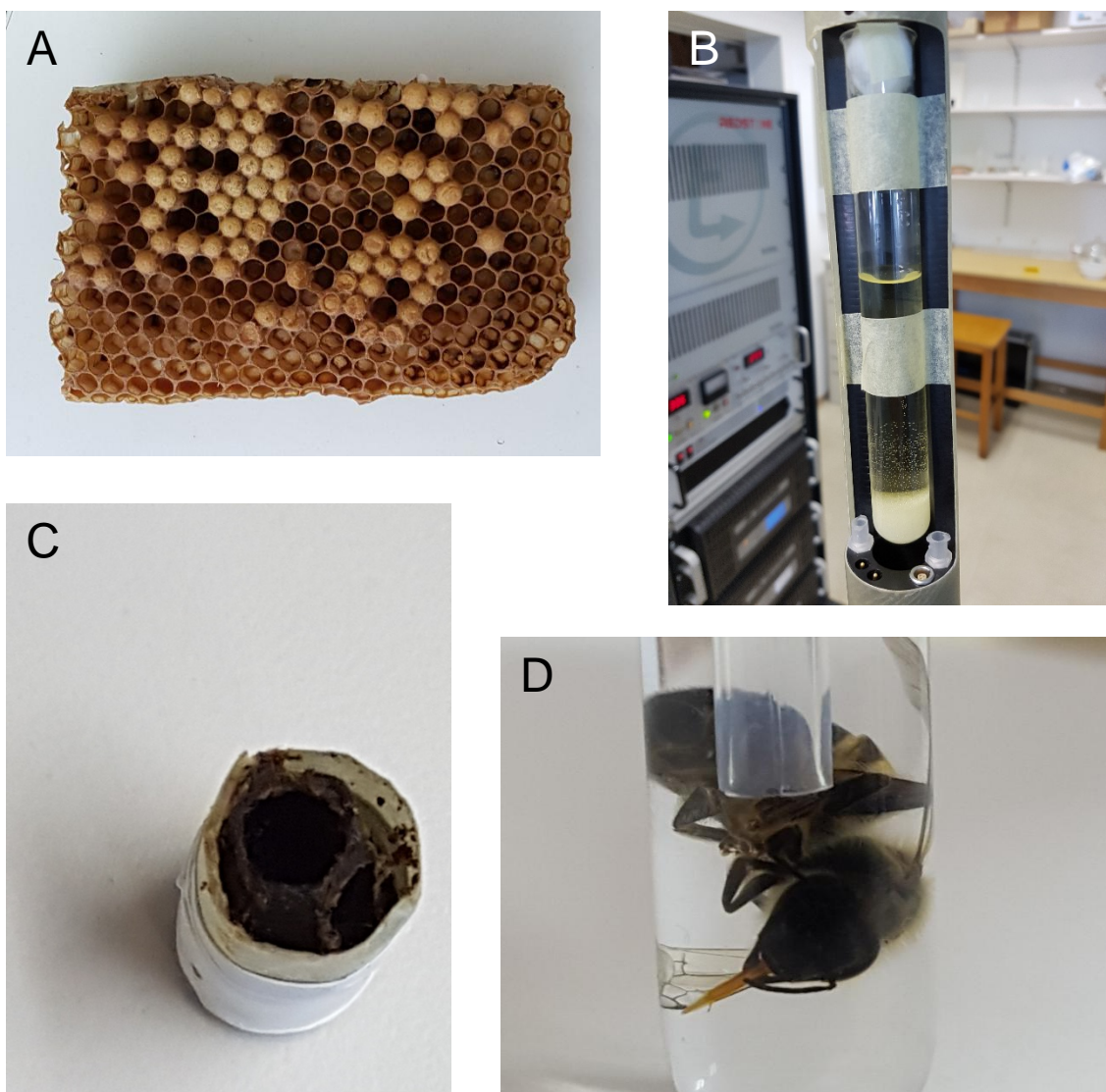
Fig. S1. Experimental setup. The experiment was performed in August 2018, which is an optimal period for bee reproduction. (A) First, a caped cell with a larva was isolated from the honeycomb. Then the cell was truncated to the diameter of 10 mm, wrapped in Teflon tape and inserted in a 10 mm probe for magnetic resonance microscopy (MRM). (B) To maintain optimal humidity of 62 % during the experiment, below the cell a tube filled with a saturated solution of $NaNO_2$ in water was placed. The optimal temperature of 34 °C was maintained during the entire experiment by the MRM probe conditioning system. (C) After twelve and a half days, metamorphosis was completed, and the adult bee emerged from the cell. (D) Adult bee emerging from the glass which was kept for further analysis.
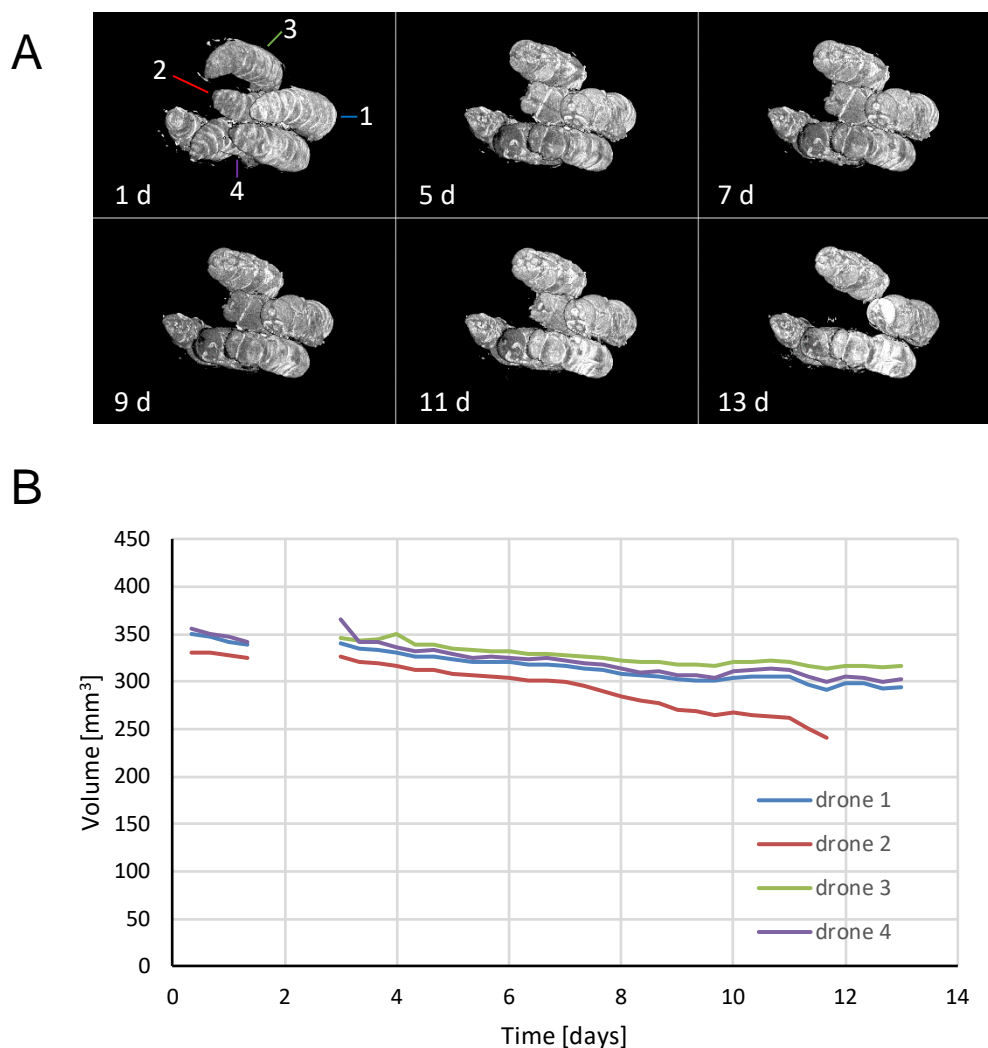
Fig. S2. Development of multiple drones followed by sequential MRM. (A) Volume rendered images of the four developing drones at different time points during metamorphosis. (B) Graph shows the total volume time courses for each of the four different drones. The analyzed drones have indices 1-4 and curves of different colors in the graph. Placing multiple specimen in the imaging field of view enables their simultaneous scanning and therefore enables the statistical analysis of variability among the specimens. This approach is much faster than the traditional approach where each specimen of the group is scanned separately. The drawback for simultaneous multiple scanning is partial loss of spatial resolution.
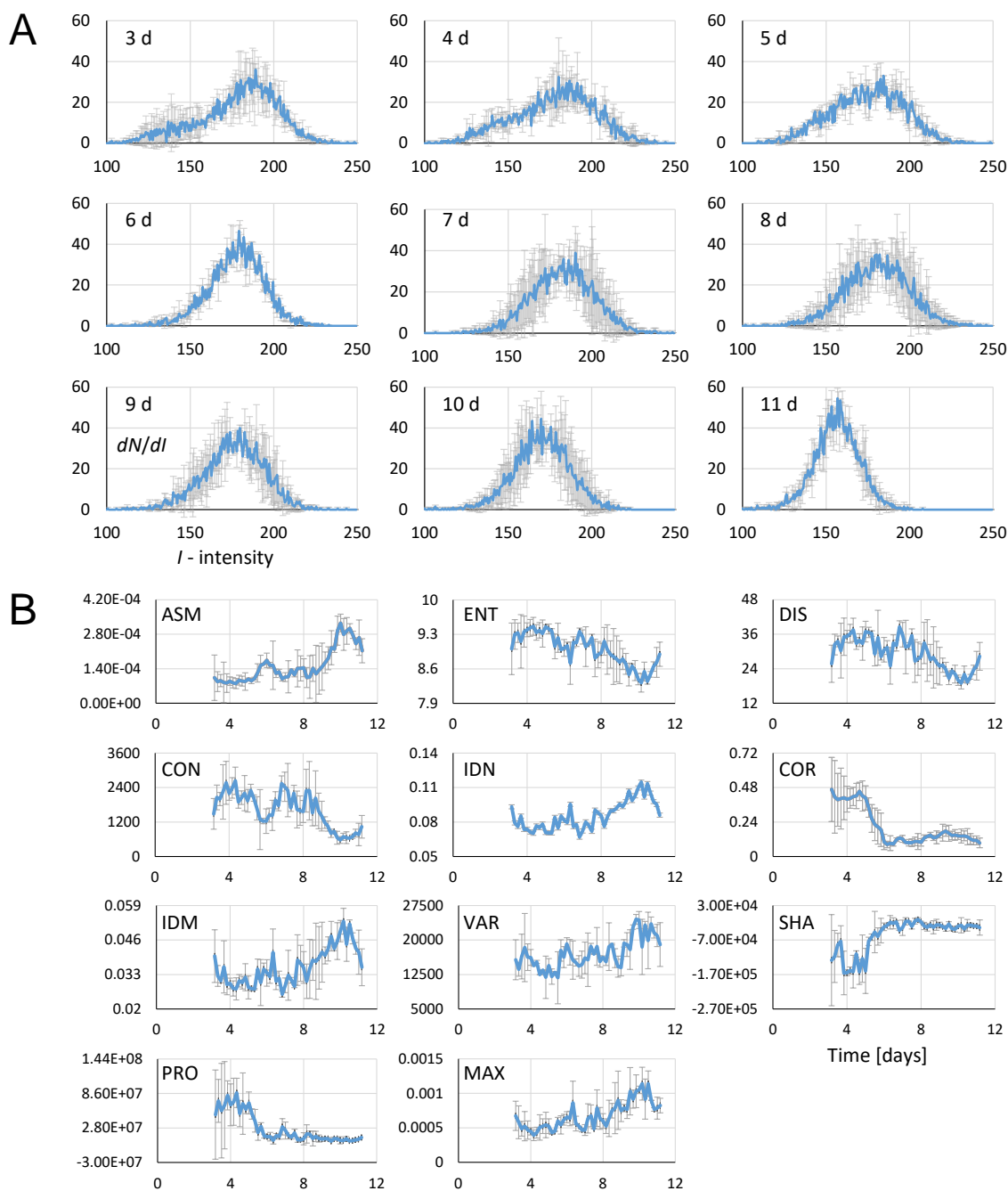
Fig. S3. Compositional analysis and structural analysis of the flight muscle. (A) The selected region of interest (ROI) within the flight muscle are analyzed by image signal histograms of both specimens at one day intervals. The histograms all exhibit approximately normal distributions; however, the distributions have different means and widths. They reveal transformation of the flight muscle composition from the initial fat-rich to the final low-fat content. (B) The selected ROI is analyzed for the structural changes by the gray level co-occurrence matrix (GLCM) analysis. Time courses of all the eleven second-order statistical texture features derived from the GLCM maps are also shown. Some of the features, such as: correlation (COR), cluster shade (SHA), cluster prominence (PRO) and angular second moment (ASM) show a marked dependence on time, while some others, e.g.: entropy (ENT), dissimilarity (DIS), contrast (CON), inverse difference normalized (IDN), inverse difference moment (IDM), variance (VAR) and maximum probability (MAX) are less distinctive.
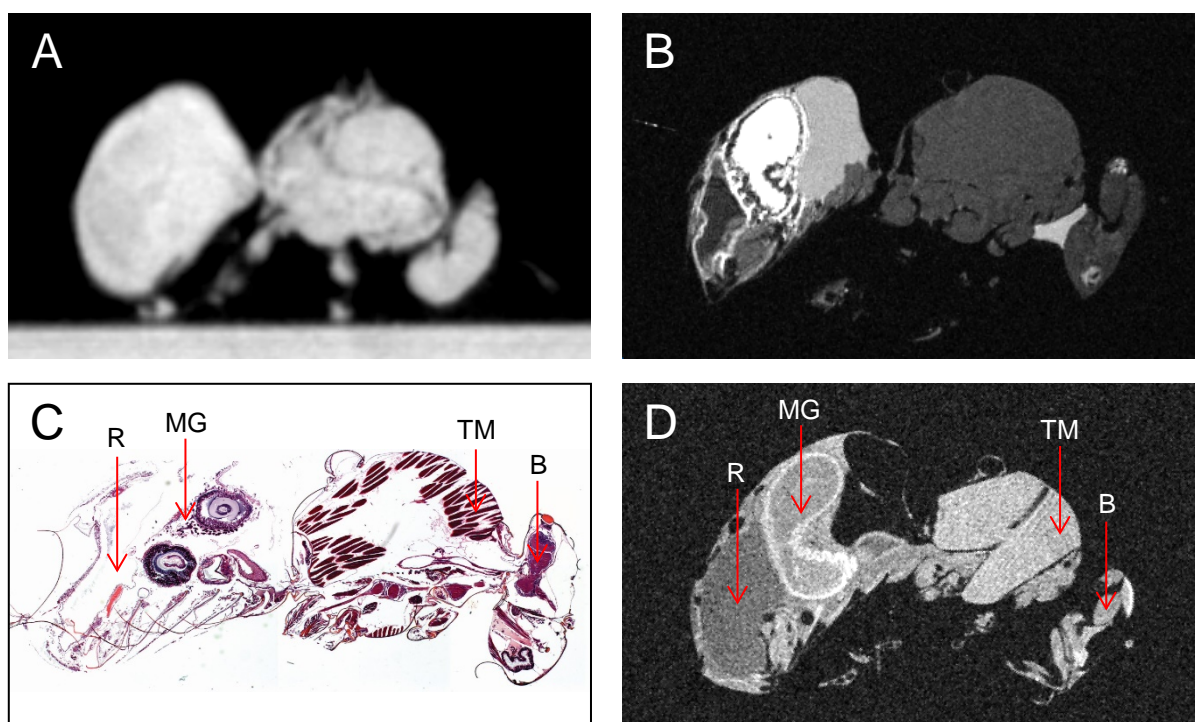
Fig. S4. Comparison between micro CT, microanatomy and MRM images. (A) micro CT and (C) microanatomical images and the corresponding MRM images of the (B) winter and (D) summer worker honey bees in identical slices. Micro CT image was acquired at field of view $40 \times 40 \times 40$ mm^3 and x-ray tube voltage was set at 90 kV, while microanatomical dissection was performed in 7 μm thick sagittal sections that were stained by hematoxylin-eosin following the procedure described in *Microanatomy* subsection. Prior to MRM scanning the samples were immersed in perfluorinated fluid (Galden SV90, Solvay, Brussels, Belgium) to prevent their desiccation during scanning which was performed using a 3D spin-echo T_1-weighetd imaging sequence with parameters TE/TR = 1.9/200 ms, field of view $18 \times 9 \times 9$ mm^3, imaging matrix of size $512 \times 256 \times 256$, four signal averages and scan time of 15 hours. Resolution of MRM images is equal to 35 μm isotropic and is equal to 80 μm in the micro CT image. Comparison of both image types clearly shows much better contrast among soft tissues in the MRM images than in the micro CT image. In the presented case the MRM images are T_1-weighetd and have tissues with higher fat content much brighter than other tissues. Due to better contrast all internal structures and organs can be better seen; it is much harder to see these on the micro CT image. Also, in terms of spatial resolution MRM images are superior and are closer to the microanatomical reference standard than the CT image. However, this is not typical as there are many reports in the literature on micro CT of insects in which approximately an order of magnitude better resolution was obtained. All major anatomical parts that are seen on the microanatomical image can be clearly seen on the corresponding MRM image as well. Specifically, brain (B) in the head, flight muscles (TM) in the thorax, midgut (MG) and rectum (R) in abdomen.
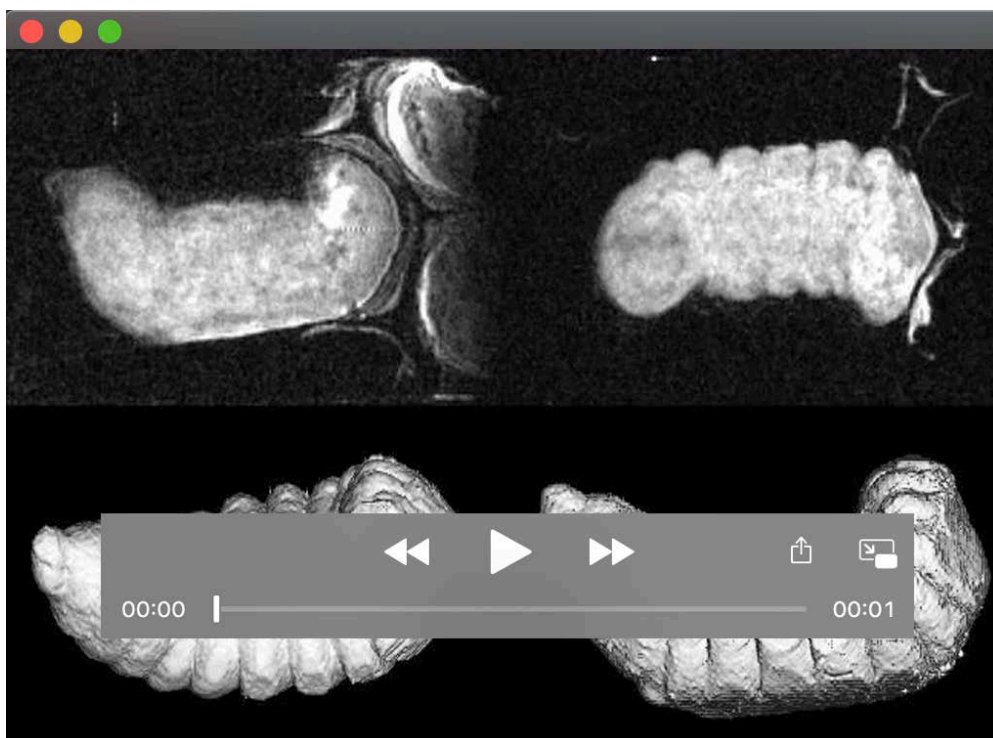
Movie 1. Metamorphosis of the bees in the central slice view and by volume-rendered images. Movies of the (left column) first and the (right column) second worker honey bee shown by: (upper row) the central slice in the sagittal orientation and by (bottom row) volume rendered images. (upper row) The central slice movies provide a clear insight into the structural changes during different stages of metamorphosis. A sudden transformation from larva to pupa was followed by the evident structural changes in the gastrointestinal tract, in the tracheal system and also in many other organs. Spatial resolution of the movies is 78 μm. Bright regions correspond to fat-rich tissues, while the darker regions contain more body fluids; signal void regions contain no tissues. Blurred frames at the end of the movies indicate intense spinning by the pupa. (bottom row) A complete set of all image slices, i.e., a full 3D image also enables the volume rendering of the entire bee. This study was done with the Fiji distribution of the ImageJ digital image processing software on each of the acquired images with the matrix size of $256 \times 128 \times 128$. The movies show worker bee metamorphosis from the sealed larva to the emergence of an adult bee.
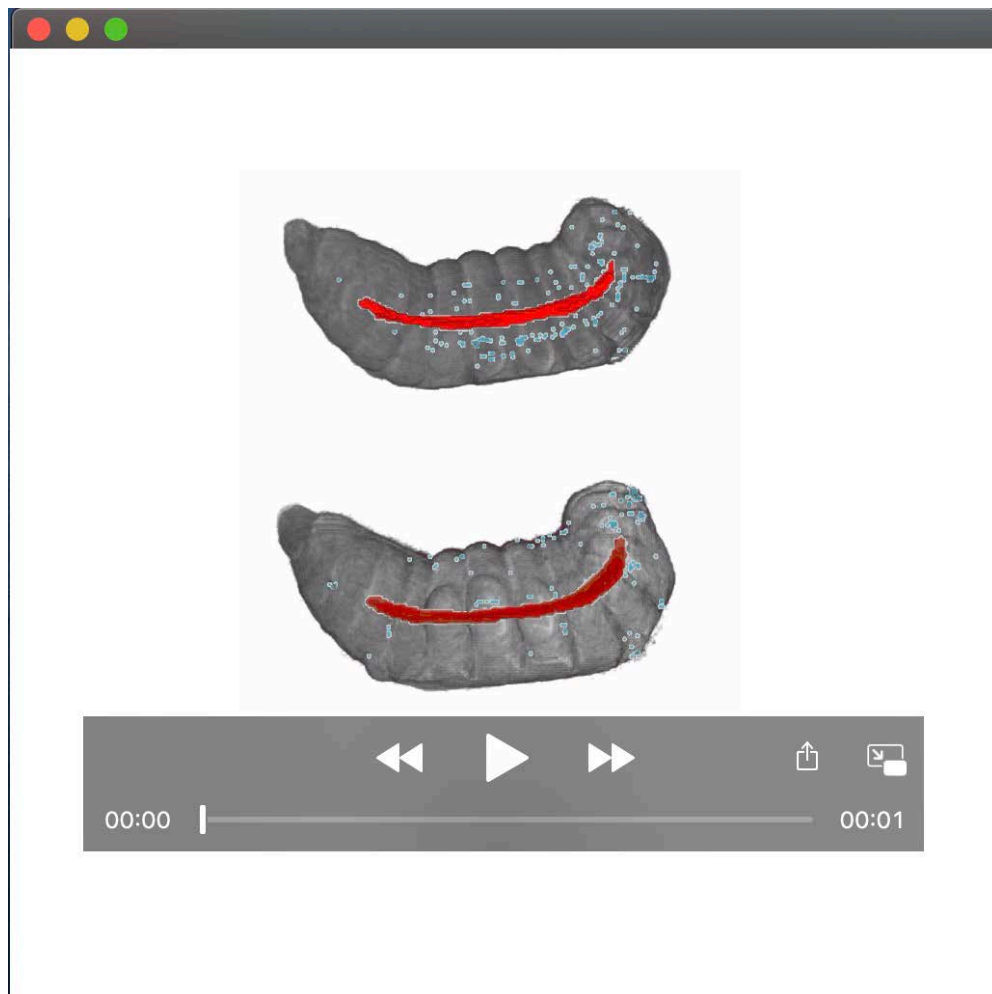
Movie 2. Development of tracheal and gastrointestinal system. Movies of (top) first and (bottom) second worker honey specimens show a time sequence of the volume-rendered images in sagittal view of the segmented organs: gastrointestinal tract is shown in red, honey stomach in orange and tracheal system in blue. In the movies, curvature development of the gastrointestinal tract is clearly visible. The tract can be reduced to a single narrow curve spanning through the entire tract region. The curve enabled measurement of the tract length time dependence as well as the measurement of the distance between the tract end points. This information was needed for the calculation of the tract's tortuosity and its time dependence during the metamorphosis that is shown in Fig 2.